Research Square

Preprints are preliminary reports that have not undergone peer review.
They should not be considered conclusive, used to inform clinical practice,
or referenced by the media as validated information.

Spectral Tunable Room Temperature Superfluorescence

Kai Han

hankai0071@nudt.edu.cn

National University of Defense Technology https://orcid.org/0000-0001-7689-5339

Hanchang Huang

National University of Defense Technology

Hao Liu

National University of Defense Technology https://orcid.org/0000-0002-8121-2333

Ye Huang

National University of Defense Technology

Mingchen Li

National University of Defense Technology

Wenda Cui

National University of Defense Technology

Changqing Song

National University of Defense Technology

Zhongjie Xu

National University of Defense Technology

Tongcheng Yu

National University of Defense Technology https://orcid.org/0000-0002-3515-1429

Chuan Guo

National University of Defense Technology

Article

Keywords:

Posted Date: July 17th, 2026

DOI: https://doi.org/10.21203/rs.3.rs-10365592/v1

License: This work is licensed under a Creative Commons Attribution 4.0 International License.
Read Full License

Additional Declarations: There is **NO** Competing Interest.

Spectral Tunable Room Temperature Superfluorescence

Hanchang Huang[1,2,3,4], Hao Liu[1,3,4*], Ye Huang[1,2,3], Mingchen Li[1,2,3], Wenda Cui[1,2,3], Changqing Song[1,2,3], Zhongjie Xu[1,2,3], Tongcheng Yu[1,2,3], Chuan Guo[1,2*], Kai Han[1,2*]

[1]College of Advanced Interdisciplinary Studies, National University of Defense Technology, Changsha, 410073, China
[2]Nanhu Laser Laboratory, National University of Defense Technology, Changsha, 410073, China
[3]Hunan Provincial Key Laboratory of High Energy Laser Technology, National University of Defense Technology, Changsha, 410073, China
[4]The two authors made equal contributions and their rankings are not distinguished.

Abstract

Superfluorescence (SF), a collective quantum phenomenon originating from correlated emitters, has historically required cryogenic temperatures or magnetic fields and been limited to narrowband Stokes-shifted emission. Although room-temperature SF has recently been realized in lanthanide-doped systems, active control over its spectral properties remains significant challenges. Here, we propose a state-entropy framework to reveal the coherence evolution and macroscopic dipole correlation in upconversion systems, providing a theoretical foundation for manipulating superradiant processes across a broad spectral range. Based on this framework, we designed an excitation strategy to decouple and regulate the distinct energy-population pathways, specifically excited-state absorption and energy transfer upconversion/cross-relaxation, in ~23 nm $NaNdF_4$ nanocrystals at

room temperature. This approach enables multi-stage upconversion superfluorescence with tunable oscillations and nanosecond to sub-microsecond lifetimes. Most importantly, it substantially extends the accessible spectral window of room-temperature UC-SF from the previously reported two orange-red bands to six distinct emission bands covering the ultraviolet to the red (384–659 nm), accompanied by a wide-gamut wavelength-synthesized color evolution. Furthermore, cascaded excitation enables real-time emission enhancement by restoring the macroscopic dipoles correlation during the SF decay phase. This work demonstrates principles that may inform future designs of on-chip ultrafast optical computing based on spectrally tunable SF with encodable photonic emission.

Introduction

Superfluorescence (SF), as a remarkable quantum optical phenomenon, arises from the self-organization and cooperative emission of an ensemble of initially incoherent quantum emitters[1,2]. When an external radiation field excites these emitters into their excited states, uncorrelated macroscopic dipole moments first emerge. Driven by intrinsic quantum fluctuations, these dipoles spontaneously develop phase coherence, culminating in an intense, ultrafast burst of radiation that constitutes the hallmark of the SF process. These mesoscopically extended coherent states[3] could be used to boost the performance of opto-electronic devices[4], high-speed optical computing[5] and enable entangled multi-photon quantum light sources[6,7].

Historically, SF has been constrained by stringent experimental prerequisites, which are most notably cryogenic temperatures[3,8,9] or strong magnetic fields[8,10,11], and has predominantly been realized through down-conversion emission processes[3,8–10]. These inherent limitations have long hindered the

integration of SF into practical nanophotonic platforms and advanced optoelectronic applications. A transformative advance on SF has recently emerged from the field of lanthanide-doped upconversion nanoparticles (UCNPs), which demonstrated room-temperature SF featuring upconversion (UC) emission with a lifetime shortened to below 50 ns[5]. This discovery signifies a twofold departure from existing systems: 1) it circumvents the inconvenient and even extreme environmental demands of conventional SF; 2) it overcomes the intrinsic microsecond-to-millisecond radiative lifetimes that have long plagued traditional upconversion luminescence (UCL). As a result, upconversion superfluorescence (UC-SF) opens a new avenue for deploying UCNPs in scenarios requiring both ultrafast emission and ambient operation. This breakthrough substantially strengthens prospects for their use in emerging technologies such as high-speed super-resolution bioimaging, fast optical storage, and ultrafast signal transduction[12–16]. Pushing the boundaries of UC-SF, Zhou et al. (2024) [17] recently achieved 912th-order dipole-coupled SF with a sub-2.5 ns lifetime in Nd^{3+}-doped nanocrystals using femtosecond excitation under normal temperature and pressure ambient conditions[17], which is a feat that underscores the potential of lanthanide systems for ultrafast quantum optics. Importantly, UC-SF operates without relying on plasmonic nanocavities or other pre-prepared structures that conventionally used to accelerate spontaneous emission. This distinguishes it from prior smart strategies that enhance emission rates via hybrid nanostructures[18,19]. Nevertheless, these strategies often introduce fabrication complexity and compromise the compact nature of the emitter system. Enabled by better understanding of ion internal transition processes, UC-SF represents a unique framework for nanoscale ultrafast quantum optics which offers a rare combination of structural simplicity and profound physical depth.

Despite these impressive advances on SF, [5,17,20,21] a critical limitation persists:

the spectral tunability of room-temperature UC-SF remains severely underdeveloped. To date, all experimental realizations of UC-SF have been confined to the same two orange-red emission bands, centered at approximately 588 and 656 nm, originating from a limited set of radiative transitions within the Nd^{3+} ion. This narrow spectral window fundamentally restricts both the fundamental understanding of coherence dynamics across different energy scales and the practical deployment of UC-SF in applications that demand multi-wavelength operation, such as optical computing of wavelength-division-multiplexed, multicolor imaging, and spectrally encoded sensing. The expansion of UC-SF into a broader spectral range (from the ultraviolet through the visible to the red) would not only provide deeper insight into the population pathways and dipole correlation mechanisms at higher-lying energy states, but would also transform UC-SF from a single-color quantum phenomenon into a versatile, spectrally-addressable photonic platform.

Moreover, a conceptual gap remains in the theoretical description of UC-SF. Recently, Kenan G. et al. proposed an explanation of SF in perovskites from the perspective of system entropy evolution, linking transient SF to equilibrium phase transitions.[22] However, this framework, developed for narrow-gap semiconductors, cannot be directly applied to $NaYF_4$-based UCNPs, which are wide-bandgap insulators with ultra-stable trivalent lanthanide ions. The physical characteristics of these materials give rise to fundamentally different mechanisms governing the emergence and evolution of macroscopic coherence, and a suitable theoretical framework for understanding and actively manipulating UC-SF in such insulating systems remains unexplored.

To address these intertwined challenges, this article studies UC-SF at room temperature, providing insight understanding and advancing its application via

designed experiments. Three pivotal contributions are as following.

Firstly, this study proposes a state-entropy framework that resolves the existing contradiction concerning the distinct kinetic pathways of macroscopic dipole formation in UC-SF[5,17]. This entropy-based mechanism can quantify the evolution of spontaneous synchronization of macroscopic dipoles, allowing us to manipulate distinct energy-population pathways, specifically excited-state absorption (ESA) and energy transfer upconversion (ETU) /cross-relaxation (CR), for programmable emission dynamics. The framework thus provides a unified theoretical basis for understanding and controlling SF processes in lanthanide-doped systems.

Firstly, this study proposes a state-entropy framework that resolves the existing contradiction concerning the distinct kinetic pathways of macroscopic dipole formation in UC-SF. This entropy-based mechanism quantifies the evolution of spontaneous synchronization of macroscopic dipoles, allowing us to manipulate distinct energy-population pathways—specifically excited-state absorption (ESA) and energy transfer upconversion/cross-relaxation (ETU/CR)—for programmable emission dynamics. The framework thus provides a unified theoretical basis for understanding and controlling SF processes in lanthanide-doped wide-bandgap insulators, a class of materials for which no such description previously existed.

Secondly, and most importantly, we achieve a dramatic spectral expansion of UC-SF that fundamentally overcomes the long-standing spectral limitation of this quantum emission system. All previous room-temperature UC-SF realizations were restricted to two emission bands in the orange-red region.[5,17] Guided by our state-entropy framework, we deliberately engineer excitation conditions that simultaneously populate multiple high-lying energy states,

thereby activating six distinct UC-SF bands spanning from 384 to 659 nm. This six-band coverage bridges the ultraviolet and the full visible spectrum, representing an unprecedented level of spectral control in room-temperature SF. Based on wavelength synthesis from these six discrete channels, we demonstrate fast-response, wide-gamut color evolution that is impossible with the previously reported two-band SF. This spectral expansion considerably extends the capability of existing SF systems.

Thirdly, grounded in the state-entropy framework, we experimentally verify that a secondary excitation pulse can revive the macroscopic dipole correlation during the SF decay phase, thereby enhancing the transient emission intensity. Leveraging this principle and the spectrally tunable UC-SF characteristics, we further demonstrate a proof-of-concept application by implementing multi-channel optical logic gates on a micron-scale emission region. This demonstration provides a principle that may inform future designs of on-chip ultrafast optical computing based on spectrally tunable UC-SF with encodable photonic emission.

Result

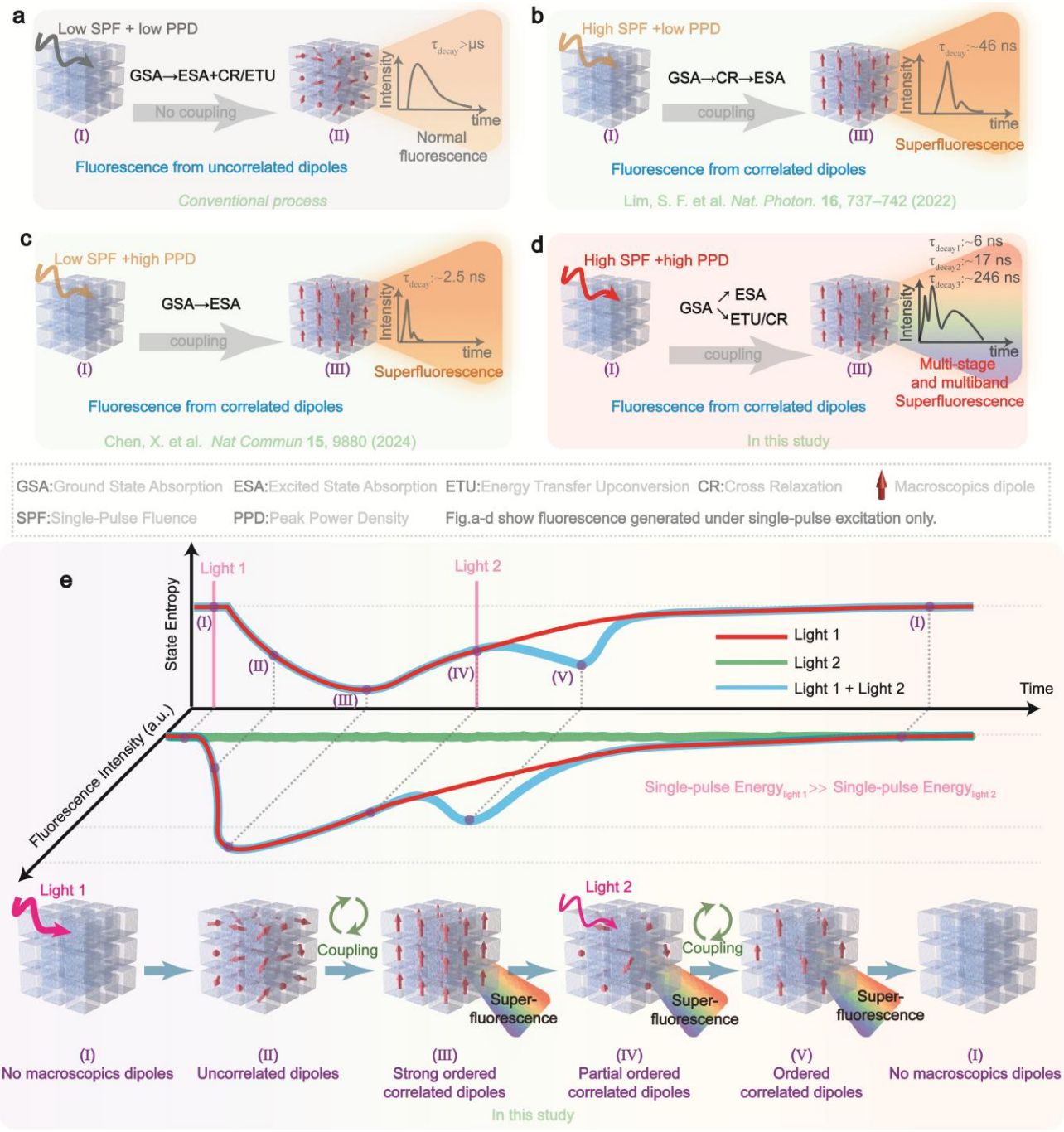

Fig. 1 (a) UCL process with a microsecond-scale lifetime, governed by GSA, ESA, and ETU/CR kinetics. (b) Lim, S.F. et al. first observed orange and red oscillatory UC-SF at room temperature, with a shortest lifetime of 46 ns and a kinetic pathway of GSA → CR → ESA.[5] (c) Chen, X. et al. achieved orange and red oscillatory UC-SF with an ultrashort lifetime of 2.5 ns using femtosecond pulses, following the kinetic pathway GSA → ESA.[17] (d) In this study, UC-SF is realized through the combined action of GSA → ESA and GSA → ETU/CR, expanding the emission wavelengths from the ultraviolet to the red and producing distinctive multi-stage oscillations in which the first peak is weaker than the second. (e) Schematic illustration of the state-entropy evolution during laser remote manipulation of SF.

The dynamics of UC-SF can be described within the framework of the Dicke model[2,17], which considers an ensemble of N identical two-level atoms (emitters). The upper and lower states of each emitter are denoted as $|e\rangle$ and $|g\rangle$, respectively. The radiative transition rate for the N-atom system is given by $W \propto [(J+M)(J-M+1)]$, where J and M represent the total angular momentum, respectively. At time t=0, each two-level atom is treated as a fictitious spin of 1/2, and all emitters are initially excited such that the total angular momentum takes the value J = N/2. Initially, when J = M = N/2, the radiative transition rate $W \propto N$, indicating that the emission starts from spontaneous emission. As time evolves, the system cascades down through energy levels with equally energy gaps, leading to a gradual increase in W from $W \propto N$ to $W \propto N^2/4$ (when M = 0). The state at M = 0 is identified as the Dicke superradiant state[1,2]. Beyond this state, the system progressively transitions from superradiance state into ordinary excited states and eventually reaches the ground state.

As illustrated in Fig. 1a, under conventional excitation conditions, Nd^{3+}-doped systems generate macroscopic dipoles through processes such as ground state absorption (GSA), ESA, and ETU/CR. However, owing to factors such as insufficient excitation power density, the phases of these macroscopic dipoles remain uncoupled. The system therefore produces ordinary UCL with a characteristic microsecond-scale lifetime, and the emission is dominated by red and orange bands. As shown in Fig. 1b, in 2022, Lim, S.F. et al. first discovered red-orange SF at room temperature in Nd^{3+}-doped systems by substantially increasing the excitation power density. In this case, the macroscopic dipoles generated through the GSA → CR → ESA pathway became phase-correlated, yielding a lifetime of ~46 ns with faint UC-SF oscillations. As presented in Fig. 1c, in 2024, Chen, X. et al. employed ultrashort femtosecond pulse excitation in Nd^{3+}-doped systems at room temperature and observed ultrashort red and orange SF with a lifetime of

~2.5 ns. Weak UC-SF oscillations were also detected in their measurements.

As shown in Figs. 1d–e, we introduce a state-entropy description for rare-earth-doped SF systems. Within this framework, the GSA → ESA and GSA → ETU/CR pathways both contribute to the generation of UC macroscopic dipoles. Both pathways increase the number of macroscopic dipoles and thereby enhance the coupling efficiency among them, which significantly reduces the state entropy of the Nd^{3+}-doped system and drives the ensemble of macroscopic dipoles toward a more ordered configuration. The state-entropy framework thus unifies the seemingly competing kinetic pathways into a single description of SF formation in rare-earth-doped systems.

Based on this framework, we further increase the peak power density compared with Fig. 1b and the excitation fluence compared with Fig. 1c. This promotes the generation of a large population of macroscopic dipoles in the Nd^{3+}-doped system and even enables their formation on multi-photon UC levels, thereby expanding the UC-SF emission from the ultraviolet to the red. At the same time, a tailored excitation strategy allows the SF produced by the two kinetically distinct population pathways, i.e., GSA → ESA and GSA → ETU/CR, to manifest as multi-stage UC-SF in the time domain, featuring a characteristic first-peak-weaker-than-second emission profile.

As further illustrated in Fig. 1e, the state–entropy description of SF indicates that the SF emission can be actively controlled by a dual-pulse excitation scheme through the modulation of macroscopic dipole correlation. The SF emission can be divided into five episodes. Episode I: The initial rare-earth-doped system contains no macroscopic dipoles. Episode II: Uncorrelated macroscopic dipoles are generated after excitation from Episode I. Episode III: The macroscopic dipoles produced in episode II become phase–correlated

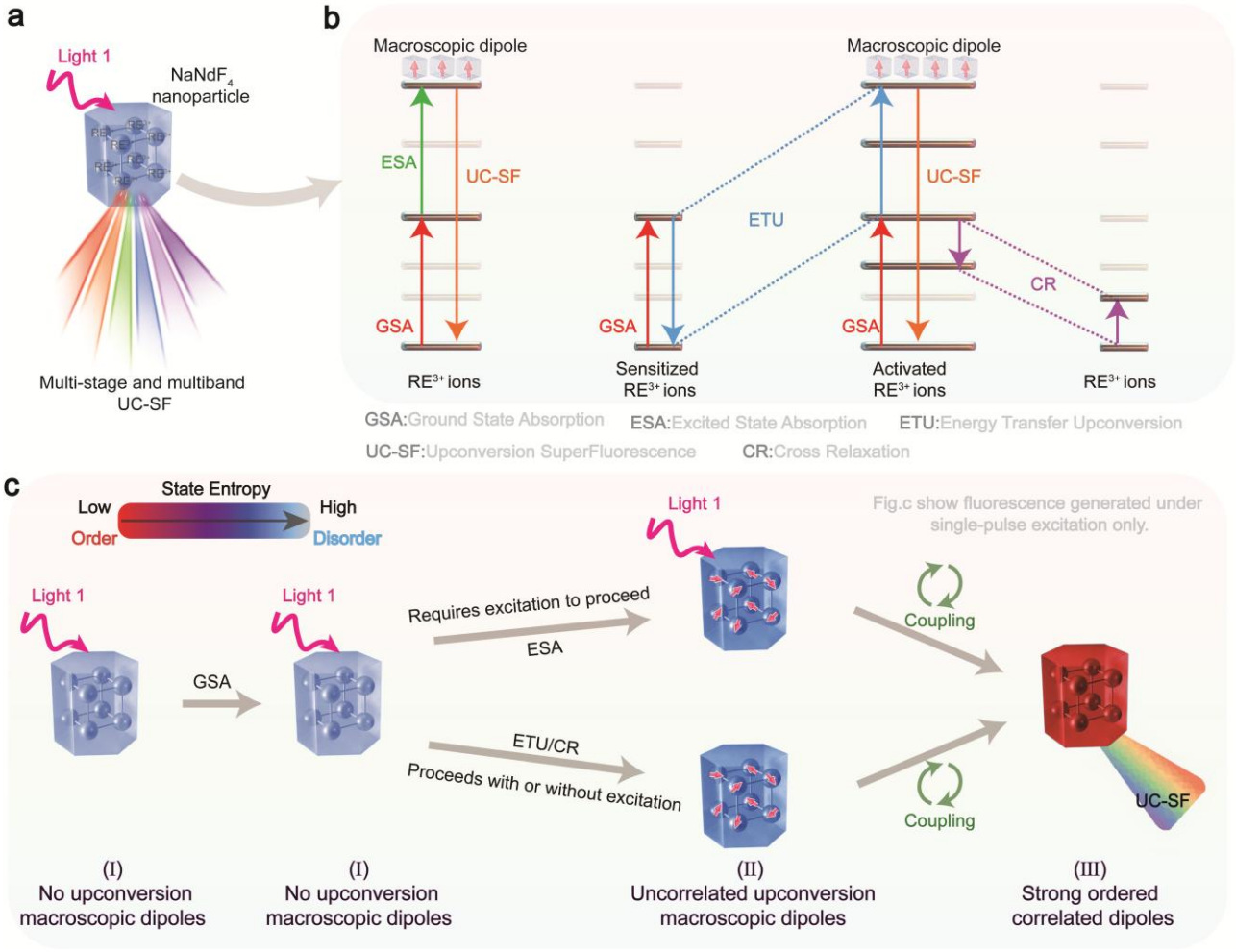

Fig. 2 (a) Schematics illustrating the multi-stage and expanded UC-SF in $NaNdF_4$ UCNPs by excitation of light 1. (b) Energy-level-based diagram of the UC dynamics. (c) Within the state-entropy framework, the kinetic process of upconversion macroscopic dipole generation in $NaNdF_4$ nanocrystals after excitation by light 1.

through spontaneous fluctuations and emit UC‐SF. Episode IV: As the emission process evolves, both the number of macroscopic dipoles and their mutual correlation decrease, leading to a decline in the UC‐SF intensity. Episode V: On the basis of episode IV, a second excitation pulse is introduced. The weak excitation of light 2 restore the phase correlation of the partially decorrelated macroscopic dipoles and enhance the emission intensity. As the emission continues, all macroscopic dipoles in the rare‐earth‐doped system are eventually depleted, and the system returns to the initial state (Episode I).

We employ $NaNdF_4$ upconversion nanocrystals (UCNPs) as the emitter system to achieve UC-SF, as schematically illustrated in Fig. 2a. Details of the

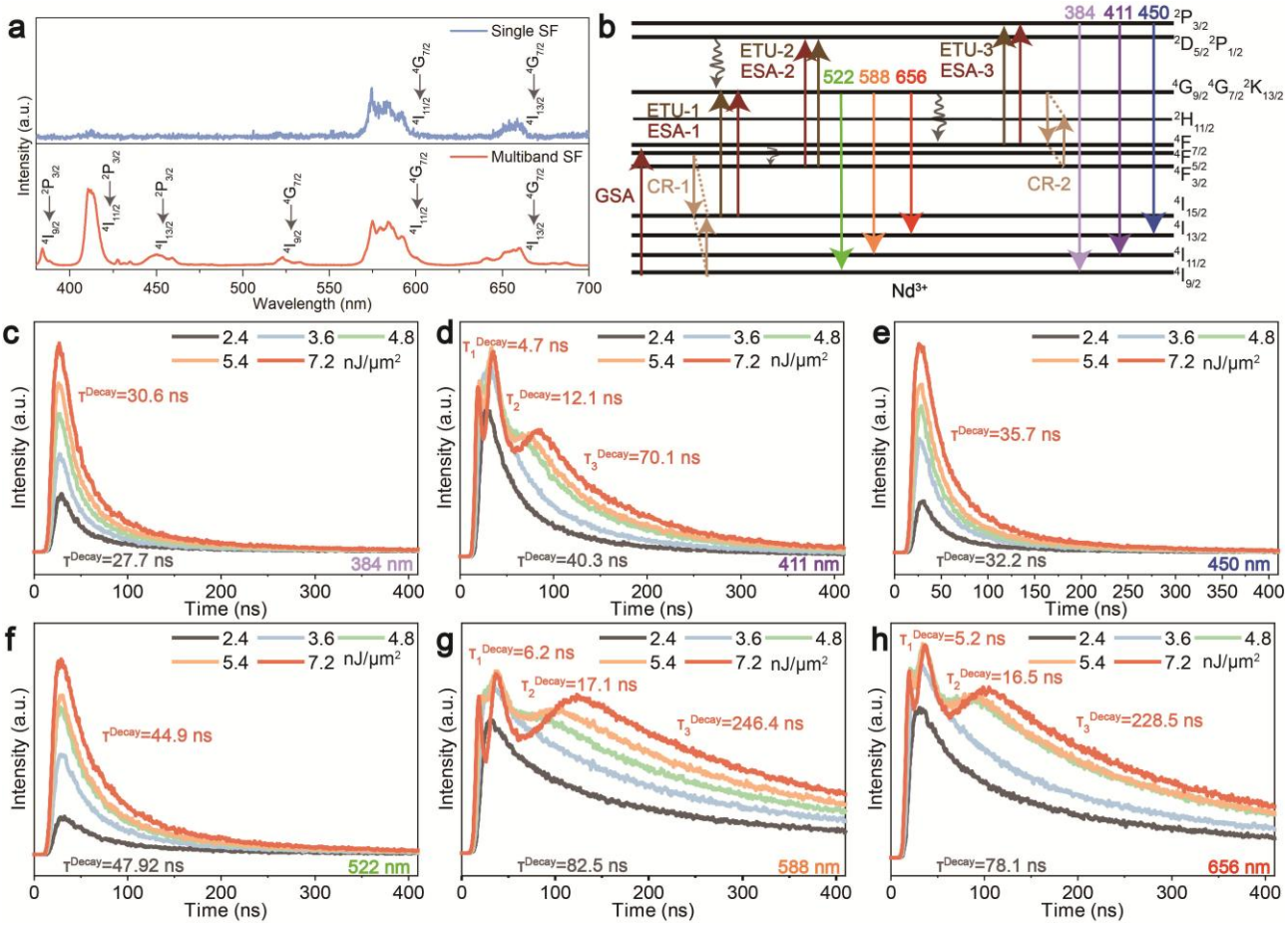

Fig. 3 Spatial resolved spectra of UC-SF emissions obtained solely by single-pulse light 1. (a) UC-SF emission spectra observed at the excitation by single pulse with low (blue line,0.06 nJ/μm^2) and high (red line, 7.2nJ/μm^2) pulse energy, showing both single-band and multi-band profiles. The integration time is 100 μs, with the zero-time set before the excitation. (b) Dynamics of energy level transitions associated with UC-SF emission. (c-h) Time-resolved UC-SF emission intensity under single-pulse light 1 by various excitation energy densities at wavelength of (c) 384, (d) 411, (e) 450, (f) 522, (g) 588, and (h) 656 nm.

sample preparation and characterization are provided in Supplementary Note 1. As shown in Fig. 2b, unlike conventional Stokes-shifted emission, UC-SF proceeds through a sequence of UC steps that accumulate population in high-lying energy states. These steps include GSA, ESA, ETU and CR. The rich dynamic processes drive Nd^{3+} ions to occupy higher energy levels, enabling the emission of photons with wavelengths shorter than that of the excitation light. Simultaneously, the large electronic population in the high-lying levels promotes the generation and mutual correlation of macroscopic dipoles, thereby triggering spectra-expanded UC-SF emission.

Recent theoretical advances on SF[22] can hardly reveal the origin of UC-SF in UCNPs directly. The reason is that, unlike the narrow-bandgap semiconductors such as perovskites used in Ref. 22, the $NaYF_4$-based UCNPs studied here are wide-bandgap insulators that contain highly stable rare-earth ions. These characteristics give rise to a distinct mechanism that calls for new physical explanations. Within the state-entropy framework, Fig. 2c illustrates the kinetic process of upconversion macroscopic dipole generation in $NaNdF_4$ nanocrystals by excitation of Laser 1. Because the transition pathways shown in Fig. 2b differ in their physical origin, the generation of upconversion dipoles exhibits pronounced spatiotemporal evolution. GSA and ESA are directly driven by the laser field, and their spatiotemporal extent is therefore restricted to the duration of the excitation pulse. In contrast, ETU and CR are governed by long-lived intermediate levels and by inter-ion distances. Consequently, they can actively redistribute energy and populate high-lying states even after the excitation pulse has ceased. This mechanism has been elaborated in our recently published work[23]. The two processes jointly promote the population of high-lying energy states and the formation of a large number of macroscopic dipoles. Subsequently, fluctuations drive these dipoles into a correlated state, reduce the state entropy, and trigger UC-SF emission (Fig. 2c, from episode I to episode III). In previous studies, these two mechanisms have rarely been combined in a single system for luminescence emission. In this work, we strategically combine them through a tailored excitation scheme that controls the transition pathways, thereby realizing UC-SF with tunable emission characteristics.

The temporal resolved spectra recorded in the experiments are shown in Fig. 3. Details of the sample characterization and experimental setup are provided in Supplementary Notes 1 and 2. The spectra of conventional UC-SF, in which the emission features arise at 588 and 656 nm, are illustrated as blue line in

Fig. 3a. The limited number of UC-SF bands in the blue spectrum results from the low per-pulse energy, which is inadequate to surpass the elevated energy thresholds for higher-level population (even with peak power intensity as high as ~30 kW/cm² when pulse energy is insufficient). Laser beam with higher pulse energy is capable to populate higher level states and activate additional transitions. As a result, the spectrum measured from higher pulse energy exciting (red curve, Fig. 3a) illustrates six emission bands centered at 384, 411, 450, 522, 588, and 656 nm. The luminescence kinetics model in Fig. 3b indicates that the shorter-wavelength emissions originate from a three-photon UC process, distinguishing them from transition processes corresponding to longer wavelength. Details of the kinetic model are provided in Supplementary Note 3.

To further explore and explain the dynamics, we investigate UC-SF intensity of each emission at its center wavelength vs. time at different laser irradiation with various energy density (Fig. 3c–h). Under low excitation energy, all UC-SF bands display tens of nanosecond-scale decay, and majority of them decay within sub-50 ns. As increasing pulse energy, the lifetimes of the bands with weak emission centered at 384, 450, and 522 nm remain almost unchanged, whereas the stronger bands at 411, 588, and 656 nm manifest obvious temporal oscillations. These results suggest there is undiscovered dynamics under high pulse energy exciting condition. These six emission wavelengths provide further experimental evidence for SF, as detailed in Supplementary Note 4.

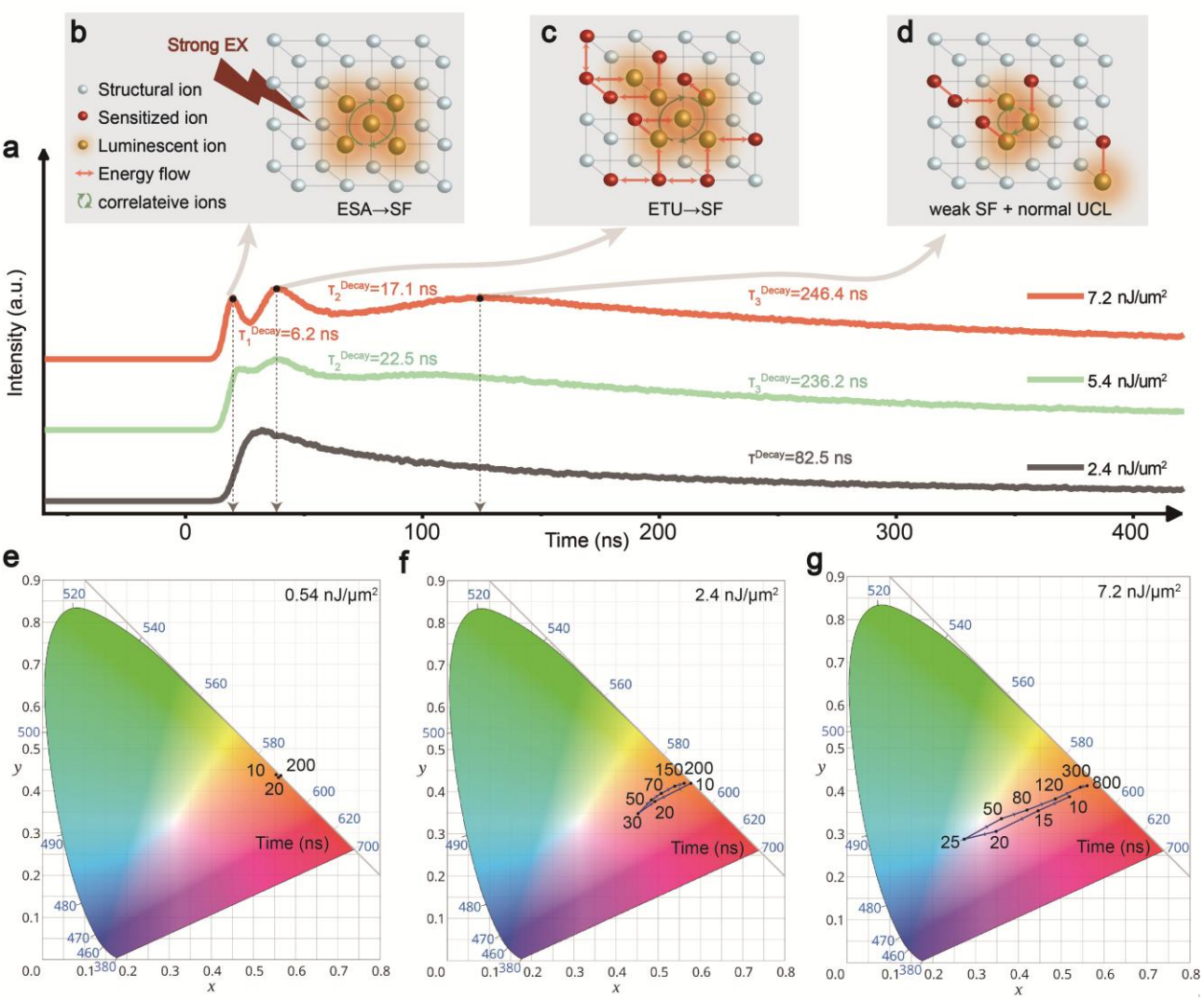

Fig. 4 Manipulable emission pathways of UC-SF and tunable color achieved solely by varying the pulse energy of light 1. (a) Temporal evolution of the 588 nm UC-SF band under varying excitation energies. (b-d) Schematics of the UC-SF formation pathways through (b) ESA and (c) ET. (d) hybrid luminescence via weak UC-SF and ordinary UCL. (e-g) Corresponding color coordinates (CIE 1931) of synthesized from the six UC-SF emission bands.

Based on analysis of Fig.3, Fig. 4a shows excitation-dependent oscillatory dynamics of UC-SF. Under low excitation energy, the time-dependent intensity profile exhibits a single maximum. As the energy increases, the dynamics transition into a tri-modal oscillatory regime, characterized by a fast (~6.2 ns decay), a dominant (~17.1 ns decay), and a slow component (~246.4 ns decay) appearing in sequence. The faster population accumulation via ESA results in quicker UC-SF emission compared to the slower ETU/CR pathway. However,

in UC systems based on Ln^{3+}, ETU/CR dominates the overall UC process. The ESA contribution is limited by the effective irradiance energy available during its characteristic transition time, and it is therefore generally weaker than the ETU/CR contribution[23,24]. As a result, UC-SF originating from ESA is difficult to observe under weak excitation, only becoming detectable under strong irradiation. Even with high irradiance, since ETU/CR remains the dominant UC mechanism, the emission peak from ESA is generally weaker than that from ETU/CR. This explains why, in multi-peak UC-SF dynamics, the first peak (associated with ESA) is less intense than the second (dominated by ETU/CR). This feature serves as a signature of oscillating UC-SF and distinguishes it from conventional SF. It originates from the temporal competition between different UC pathways within the UC-SF mechanism. The rapid rise of the first peak in the experimentally measured spectra in Fig. 4a agrees with the theoretical explanation given above and confirms that ESA dominates the first fast peak emission. Furthermore, the proposed ESA mechanism can also account for the sub-2.5 ns UC-SF excited by femtosecond pulses as reported by Zhou *et al.*[17] Although ETU is the predominant UC mechanism in lanthanides, increasing the peak irradiance specifically enhances the ESA pathway.[23] Being synchronous with the excitation, the ESA-induced first peak consequently shifts earlier as the power density increases.

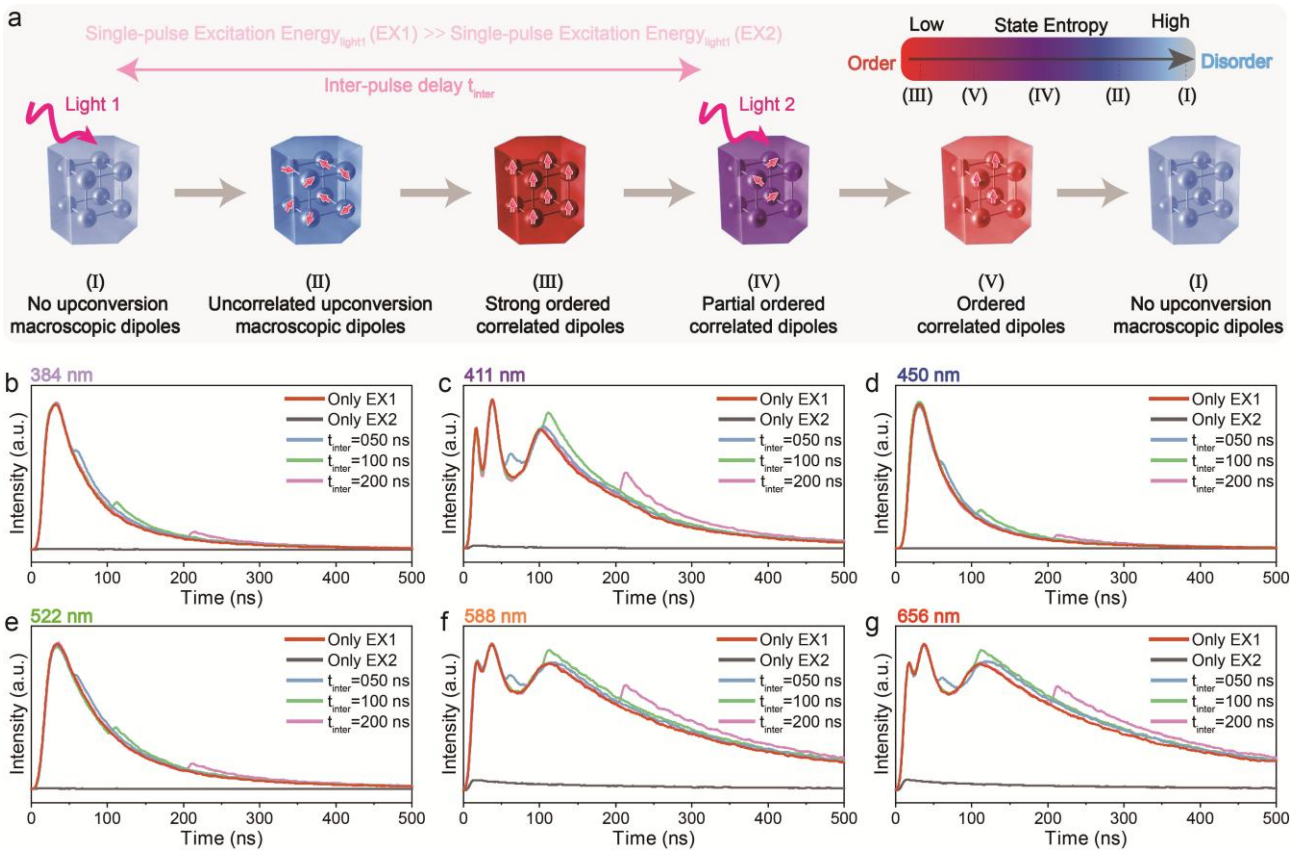

Fig. 5 (a) Schematic illustration of the dual-pulse-manipulating UC-SF. EX1 has a fluence of 7.2 nJ/μm² and EX2 a fluence of 0.54 nJ/μm². (b–g) Temporal evolution of the emission intensity at different wavelengths under dual-pulse excitation: (b) 384 nm, (c) 411 nm, (d) 450 nm, (e) 522 nm, (f) 588 nm, and (g) 656 nm.

The second principal peak arises from ETU processes between lanthanide ions (Fig. 4c), exhibiting a distinct temporal signature governed by ion spatial distribution. Its appearance time is stable against energy variations once the excitation energy passes its threshold. As the main UC mechanism, the peak generated by the ETU process is the most intense. Especially, the ESA is weak under low irradiance and ETU takes the dominant position. The slower population rate of ETU, constrained by the spatial energy migration time, delays this peak relative to the ESA peak. This slower build-up also diminishes macroscopic dipole correlation, explaining the subsequently slower decay (lifetime ~17.1 ns) of the ETU-induced UC-SF compared to its ESA.

Because the UC-SF oscillatory dynamics depend on the excitation fluence,

varying the single-pulse energy effectively tunes the wavelength-synthesized emission color (Figs. 4e–g). The color is limited to a persistent red-orange at low energy and struggles to escape this dominance at intermediate levels. However, at 7.2 nJ/μm², the system exhibits tunable color, traversing color field of orange→white→blue, thereby enabling broad gamut emission control. Details of wavelength-synthesized are provided in Supplementary Note 6.

During the third emission peak, as shown in Fig. 5a, the decline in macroscopic dipole correlation is a crucial factor leading to the reduced radiation rate in UC-SF, regardless of whether it was initially generated via ESA or ETU. Introducing a low-energy laser pulse at this episode can promote coupling between the remaining macroscopic dipoles, thereby reviving superradiant state of the system. When the weak pulse (light 2) is applied after a delay t_{inter} following a strong excitation (light 1), a significant signal enhancement is clearly observed. Physically, after the first two UC-SF peaks, the state entropy increases, resulting in greater disorder and reduced dipole correlation. The weak laser pulse (light 2) effectively reduce the state entropy, enhance dipole correlation, increase the radiation rate, and thus amplify the UC-SF intensity.

The above experiment demonstrates that two lasers can externally regulate the spectral and temporal evolution of UC-SF. Benefiting from this newly discovered tunable UC-SF phenomenon, we demonstrated a proof-of-concept logic gate operation using a nanocrystal aggregate. In the experiment, two laser beams (I_1 and I_2) served as the input signals, while six distinct UC-SF spectral bands functioned as the output channels, as detailed in Supplementary Note 5. Owing to their synchronous computing capability, these logic gates may serve as a promising and universal platform for optical logic, paving the way for future high-speed optical computing and related advanced

applications.

Discussion

This study elucidates the intricate mechanism of UC-SF at room temperature and advances its external control. It proposes a state-entropy theoretical framework and demonstrates enhanced manipulability in both transition pathways and spectrally-temporally resolved emission. Unlike previous SF systems that are constrained by cryogenic temperatures or limited spectral tunability, our work establishes $NaNdF_4$ nanocrystals as a versatile platform for encodable photonic emission at room temperature without requiring pre-fabricated nanostructure (e.g. nanocavity, core-shell structure, etc.). The key advance lies in the decoupling and regulation of distinct energy-population pathways, namely ESA and ETU/CR, through a designed excitation strategy. This enables multi-stage oscillatory UC-SF with lifetimes ranging from nanoseconds to sub-microseconds. Most importantly, it substantially expands the spectral range of room temperature SF from the two orange red bands reported previously to six distinct bands covering the ultraviolet to the red region, accompanied by a wide gamut wavelength synthesized color evolution. Such programmable UC-SF in both temporal and spectral dimensions reveals a behavior previously unreported in UC or SF systems, and highlights the distinctive nature of the present UC-SF system.

From theoretical perspective, a central insight afforded here lies in the role of proposed state-entropy mediating macroscopic dipole correlation. Our state-entropy framework provides better understanding for SF phenomena. Recent studies, such as Ref. 22, reported SF in narrow gap semiconductors by linking it to equilibrium phase transitions. However, that model cannot directly account for the mechanisms in wide bandgap insulators like $NaYF_4$ based

nanocrystals. The present entropy-based approach coherently interprets the spontaneous synchronization and dephasing of macroscopic dipoles in lanthanide systems. It highlights how entropy reduction during phase synchronization leads to superradiant bursts, while entropy increase drives decay: a process reversibly modulated by correlated photon pulses. This framework not only explains our observations of multi-peak oscillations and emission recovery but also bridges the gap between perovskite-based SF and lanthanide-based UC-SF. More importantly, it offers physical mechanism basis for manipulating transition pathways and designing encodable nanoscale emission sources in this study.

From an experimental perspective, the observation of triple-peaked UC-SF oscillations reveals a temporal competition between population-building mechanisms under high pump fluence. These oscillations comprise a fast ESA-dominated peak with a decay of ~6.2 ns, a dominant ETU/CR-driven peak with a decay of ~17.1 ns, and a slow collective decay peak with a decay of ~246.4 ns.

This multi-stage behavior, absent in existing SF systems[5,17,21,22,31], underscores the uniqueness of lanthanide platforms where long-lived intermediate states facilitate post-excitation energy redistribution. By varying the excitation energy, we achieved six distinct emission bands at 384, 411, 450, 522, 588, and 656 nm. This spectral expansion is a central result of our study. It enables rapid color switching by wavelength-synthesized on nanosecond timescales, such as from orange to white to blue. Such spectral and dynamic tunability is superior to the capabilities of prior room-temperature SF works, which often exhibit limited color ranges or spectral profiles. Furthermore, the real-time enhancement of UC-SF intensity via a secondary weak pulse during the decay phase exemplifies active correlation control, reducing state entropy to revive superradiance, which are not demonstrated in earlier studies. The

restoration of the superradiant state by secondary excitation also serves as an important reference for enhancing luminescence emission under high-repetition-rate operation beyond10MHz.

The practical implications of these experimental findings are notable, as evidenced above by the proof-of-concept demonstration of optical logic gates at the on a micron-scale emission region (as detailed in Supplementary Note 5). Leveraging multi-color UC-SF channels, we enabled simultaneous logic operations highlighting potential for ultrafast, synchronous photonic computing architectures. This provides potential approach toward tangible applications, such as on-chip photonic computing, high-speed optical displays, information encryption, etc., where minimal spatial footprint and external manipulable operation are critical. Previous SF systems rely on pre-fabricated nanostructures or extreme conditions (e.g. fs laser excitation, low temperature), while our approach emphasizes intrinsic physics properties and excitation engineering, simplifying integration into on-chip devices, therefore, capable to serve as a general platform that requires photonic manipulations[25,27–30,32].

Materials and methods

Materials and Preparation

β-$NaNdF_4$ nanocrystals were synthesized using a co-precipitation approach. First,1 mmol $NdCl_3 \cdot 6H_2O$ were accurately weighed and combined with 6 mL of oleic acid and 15 mL of 1-octadecene in a three-necked flask. The mixture was heated to 160 °C under argon atmosphere and maintained at this temperature for 1 h until a clear and transparent solution was obtained. Subsequently, 4 mmol NH_4F and 2.5 mmol NaOH were dissolved in 10 mL of methanol. After the reaction mixture was cooled to room temperature, the methanolic solution was added dropwise under vigorous stirring and allowed to react for 1 h at

room temperature. The temperature was then raised to 60 °C and held for 1 h to completely remove methanol. After full evaporation of methanol, the temperature was increased to 300 °C and maintained for 1 h to facilitate crystal growth. Finally, the resulting nanocrystals were cooled to room temperature, collected by centrifugation, and washed several times with a mixture of anhydrous ethanol and cyclohexane. The purified product was redispersed in cyclohexane and stored for further use.

Characterization

The β-$NaNdF_4$ UCNPs were analyzed using SEM, showing a particle size of around 23 nm (Fig.S1). XRD patterns of these UCNPs were obtained with a Cu Kα - ray diffractometer (Rigaku, 40 kV, 200 mA). XRD data were collected at a scan rate of 10°/min. The results indicate that the prepared β-$NaNdF_4$ UCNPs have a β-phase crystal structure, consistent with powder diffraction file (Fig.S2). Further details are provided in Supplementary Note 1.

Photoluminescence measurements

The equipment schematic diagram is shown in Fig. S3. A color CMOS camera, an ICCD camera coupled to a spectrometer, and a photomultiplier tube (PMT)-based single-photon counting detection system equipped with a monochromator were employed to monitor the UCNPs and collect time-resolved spectral signals. The setup incorporates two independently controlled 808 nm nanosecond pulsed excitation sources (Light 1: pulse width ~20 ns; Light 2: pulse width ~5 ns; repetition rate: 100 Hz for both). A digital delay generator (DDG) synchronizes all optical detection and excitation events, with timing calibrated using a photodiode, oscilloscope, PMT and ICCD. Both excitation beams were co-focused onto the same sample spot via a 100×

oil-immersion objective and aligned using CMOS-based micro-imaging. Further details are provided in Supplementary Note 2.

Acknowledgements

This work was supported by National Key Research and Development Program of China. (No.2023YFB3610901), the National Natural Science Foundation of China (Nos. U24B20138 and 662272421), and the Hunan Natural Science Fund for Distinguished Young Scholars (No. 2024JJ4044). The authors are thankful to Xi'an ruixi Biological Technology Co., Ltd for providing the $NaYF_4:Nd^{3+}$ UCNPs. The authors sincerely thank Prof. Hui Jing for his insightful guidance on this work.

Author contributions

H.H., H.L., C.G., and K.H. conceived the idea and initiated the project. H.H., H.L., C.G., Y.H. and M.L. designed the experiments and supervised the project. T.Y., W.C, and C.S characterized the sample. H.H., H.L., Z.X. and Y.H. analyzed the experimental results. H.H., H.L. and K.H. wrote the manuscript.

Data availability

The data that support the findings of this study are available from the corresponding author upon reasonable request

Conflict of interest

The authors declare no competing interests.

Reference

1. Bonifacio, R. & Lugiato, L. A. Cooperative radiation processes in two-level systems: superfluorescence. *Phys. Rev. A* **11**, 1506-1520 (1975).
2. R. H. DICKE. Coherence in spontaneous radiation processes. *Phys. Rev.* **93**, 99-110 (1953).
3. Rainò, G. et al. Superfluorescence from lead halide perovskite quantum dot superlattices. *Nature* **563**, 671–675 (2018).
4. Kagan, C. R. & Murray, C. B. Charge transport in strongly coupled quantum dot solids. *Nat. Nanotechnol.* **10**, 1013–1026 (2015).
5. Huang, K. et al. Room-temperature upconverted superfluorescence. *Nat. Photon.* **16**, 737–742 (2022).
6. Afek, I., Ambar, O. & Silberberg, Y. High-NOON states by mixing quantum and classical light. *Science* **328**, 879–881 (2010).
7. Muñoz, C. S. et al. Emitters of N-photon bundles. *Nat. Photon.* **8**, 550–555 (2014).
8. Cherniukh, I. et al. Perovskite-type superlattices from lead halide perovskite nanocubes. *Nature* **593**, 535–542 (2021).
9. Findik, G. et al. High-temperature superfluorescence in methyl ammonium lead iodide. *Nat. Photon.* **15**, 676–680 (2021).
10. Timothy Noe Ii, G. et al. Giant superfluorescent bursts from a semiconductor magneto-plasma. *Nat. Phys.* **8**, 219–224 (2012).
11. Rainò, G. et al. Superfluorescence from lead halide perovskite quantum dot superlattices. *Nature* **563**, 671–675 (2018).
12. Pelton, M. Modified spontaneous emission in nanophotonic structures. *Nature Photon* **9**, 427–435 (2015).
13. Liu, Y. et al. Amplified stimulated emission in upconversion nanoparticles for super-resolution nanoscopy. *Nature* **543**, 229–233 (2017).
14. Lee, C. et al. Giant nonlinear optical responses from photon-avalanching nanoparticles. *Nature* **589**, 230–235 (2021).

15. Shan, X. et al. Optical tweezers beyond refractive index mismatch using highly doped upconversion nanoparticles. *Nat. Nanotechnol.* **16**, 531–537 (2021).
16. Zhang, M. et al. Lanthanide-doped $KMgF_3$ upconversion nanoparticles for photon avalanche luminescence with giant nonlinearities. *Nano Lett.* **23**, 8576-8584 (2023).
17. Zhou, M. et al. Ultrafast upconversion superfluorescence with a sub-2.5 ns lifetime at room temperature. *Nat Commun* **15**, 9880 (2024).
18. Chen, H. et al. Sub-50-ns ultrafast upconversion luminescence of a rare-earth-doped nanoparticle. *Nat. Photon.* **16**, 651–657 (2022).
19. Wu, Y. et al. Upconversion superburst with sub-2 μs lifetime. *Nat. Nanotechnol.* **14**, 1110–1115 (2019).
20. Aggarwal, N. et al. Room temperature superfluorescence from an Electron-Hole Liquid. *Phys. Rev. Lett.* **134**, 083801 (2025).
21. Biliroglu, M. et al. Room-temperature superfluorescence in hybrid perovskites and its origins. *Nat. Photon.* **16**, 324–329 (2022).
22. Biliroglu, M. et al. Unconventional solitonic high-temperature superfluorescence from perovskites. *Nature* **642**, 71–77 (2025).
23. Huang, H. et al. Temporal evolution kinetics of upconversion population distribution resulting in transient luminescence Enhancement. *Laser photonics rev.* **n/a**, e00962 (2025).
24. Huang, H. et al. Nanosecond kinetics of multiphoton upconversion in an optically trapped single microcrystal. *J. Mater. Chem. C* **10**, 9208–9215 (2022).
25. Wetzstein, G. et al. Inference in artificial intelligence with deep optics and photonics. *Nature* **588**, 39–47 (2020).
26. Liu, H. et al. Multispectral non-line-of-sight imaging via deep fusion photography. *Sci. China Inform. Sci.* **68**, 140407 (2025).
27. Wu, J., Ji, N. & Tsia, K. K. Speed scaling in multiphoton fluorescence

microscopy. *Nat. Photon.* **15**, 800–812 (2021).

28. Tsao, C. et al. Enhancing spectroscopy and microscopy with emerging methods in photon correlation and quantum illumination. *Nat. Nanotechnol.* **20**, 1001–1016 (2025).
29. Li, C. et al. Luminescence lifetime thermometers based on hybrid cuprous halides with exceptional water resistance and giant thermal expansion. *Light Sci. Appl.* **14**, 224 (2025).
30. Gong, J. et al. Unveiling the Excited‐State Dynamics and Interfacial Interactions in Dye‐Sensitized $NaNdF_4$ Nanoparticles for Efficient Photothermal Effect. *Adv. Sci.* **12**, 2503110 (2025).
31. Mao, D. et al. Observation of transition from superfluorescence to polariton condensation in $CsPbBr_3$ quantum dots film. *Light Sci. Appl.* **13**, 34 (2024).
32. Ekim, U., Özkutay, D. et al. Full-color dynamic volumetric displays with tunable upconversion emission from RE^{3+}-doped glasses (RE = Ho, Tm, Nd, Yb) under NIR laser excitation. *Light Sci. Appl.* **14**, 15 (2025).

Supplementary Files

This is a list of supplementary files associated with this preprint. Click to download.

- Supplementaryinformation.pdf